Applied Catalysis B: Environmental 253 (2019) 300–308

Contents lists available at ScienceDirect

Applied Catalysis B: Environmental

journal homepage: www.elsevier.com/locate/apcatb

FeCo-N-C oxygen reduction electrocatalysts: Activity of the different compounds produced during the synthesis *via* pyrolysis

N.A. Galiote, F.E.R. Oliveira, F.H.B. Lima*

Instituto de Química de São Carlos (IQSC), Universidade de São Paulo, Av. Trabalhador São, Carlense, 400 CP 780, São Carlos, SP, Brazil

ARTICLE INFO

Keywords:
Oxygen reduction
Earth-abundant oxygen reduction electrocatalysts
Fuel cell cathode

ABSTRACT

During the synthesis of earth-abundant oxygen reduction reaction (ORR) electrocatalysts formed by metal, nitrogen and carbon *via* pyrolysis, a variety of side products arise in addition to the intended structure of nitrogen-coordinated metal inserted on a carbon matrix (M-N-C). In this study, some of these side products, such as nitrogen-doped carbon and carbon-encapsulated metal nanoparticles were selectively synthesized, and their electrocatalytic activities for the ORR were measured in acid and alkaline electrolytes. The ORR polarization curves showed that carbon-encapsulated iron-cobalt nanoparticles do not present an increased activity in relation to pure carbon. When the surfaces of these encapsulated nanoparticles were doped with nitrogen using thermal treatment in N_2 or in NH_3, the resulting ORR curves presented a slight shift of the onset potentials to higher values in both electrolytes. Remarkably, when a nitrogen-rich molecule (imidazole) was used as the nitrogen precursor, the highest ORR activity was achieved in both media. Only for those materials thermally treated in N_2 or in NH_3 atmosphere or synthesized in the presence of imidazole, the EXAFS characterization revealed the occurrence of iron-nitrogen and cobalt-nitrogen bonds, this being an indicative of the formation of M-N-C species. The presence of imidazole may lead to Fe and Co complexation during the first step of the synthesis, permitting better dispersion of the metallic atoms on the carbon powder, favoring the formation of M-N-C to a higher extent. Therefore, the results disclosed herein pointed out that carbon-encapsulated metal nanoparticles or even nitrogen-doped carbon-encapsulated metal nanoparticle cannot be responsible for the high half-wave potentials encountered in polarization curves for the ORR in M-N-C materials synthesized *via* pyrolysis. Only M-N-C species, even being present at low amounts, can result in high ORR activity whether in acid or alkaline media.

1. Introduction

To avoid an energy shortcoming in a near-future due to the increase of its demand, an improvement in the efficiency of energy conversion and storage devices are needed, mainly for those powered by fuels originated from renewable sources [1,2]. Among the energy converters, low-temperature proton exchange membrane fuel cells (LT-PEM) are attracting the attention of the scientific community mainly for the application in portable electronic devices and in vehicles [3–5]. Despite the improvements that have been achieved during the past few years, the oxygen reduction reaction (ORR), that takes place in the cathode of fuel cells, is still a bottleneck for developing those systems in large scale. This fact is associated with the ORR sluggish kinetics, demanding the use of high active electrocatalysts, commonly formed by noble metals (to date, platinum and platinum-alloys are the most active electrocatalysts) [2,6]. The use of noble metal-based materials elevates the overall cost of fuel cells due to their scarcity in the Earth' crust and, so, the research focused on Pt-based PEM should to be directed to the reduction of the noble metal loadings [3]. An additional problem is related to the low tolerance of noble metals to the presence of liquids fuels in the cathode compartment, if the crossover phenomenon takes place, this being the case for direct alcohol fuel cells [7].

In this scenario, different types of non-noble metal electrocatalysts have been investigated for the PEM cathode. In 1964, Jasinski studied cobalt phthalocyanines as electrocatalysts for the ORR in alkaline media [8]. However, due to the protonation of the nitrogen groups, with consequent dissolution, these phthalocyanines were unstable in strong acidic electrolytes, and studies were concentrated in alkaline media. Later, some improvements were achieved by pyrolyzing the macrocycles or using iron or cobalt complexes with non-macrocycles ligands. This procedure resulted in the formation of M-N_4-C moieties, similar to those presented in the central part of porphyrins and

* Corresponding author.
E-mail address: fabiohbl@iqsc.usp.br (F.H.B. Lima).

https://doi.org/10.1016/j.apcatb.2019.04.057
Received 18 October 2018; Received in revised form 27 March 2019; Accepted 17 April 2019
Available online 19 April 2019
0926-3373/

phthalocyanines, and, additionally, produced materials are much more resistant against proton corrosion and, so, capable to operate in acidic electrolytes [9,10].

For this type of ORR electrocatalyst, there is a consensus that small changes in the synthesis parameters such as pyrolysis temperature, metal valence/nature, carbon type, and nitrogen precursor, result in different ORR activities [2,7,11]. In addition, several different compounds such as metal nitrides, oxides, carbides, and carbon-encapsulated metal nanoparticles (M@C) structures that are formed during the high-temperature pyrolysis step, in addition to the desired nitrogen-coordinated metal atoms inserted on a carbon matrix (M-N-C) species [2,12,13,14–19]. This is an important obstacle that decelerates the complete understanding of the parameters the govern the electrocatalytic activity of M-N-C electrocatalysts and, therefore, hinders to development of reproducible and better electrocatalysts. Some authors claim that, among the different kind of structures, only the M-N-C species are highly active towards the ORR [1,7,14,15,20–26]. Additionally, for M-N-C, a synergistic effect has been evidenced for bimetallic electrocatalysts, resulting in more active and more stable materials for the ORR [23,27–29]. For those bimetallic materials, with dual active sites (usually represented by M1M2-N-C), mainly for those formed by the combination of Fe and Co [29], it was shown that the energy barrier for the O—O bond breaking is lowered, which increases the ORR rate. Therefore, these dual sites lead to a reduced H_2O_2 formation, as evidenced by rotating ring-disk measurements [28]. Thus, it is likely that the arrangement (or location) of the Fe and Co atoms in the electrocatalyst structure is an important factor governing the activity and stability. Interestingly, and in contrast to what was mentioned above, some authors claim that the encapsulated nanoparticles are also highly active towards the ORR in both acid and alkaline media [14,24,30]. For example, Mukerjee et al. [31] proposed that these metal nanoparticles boost the activity of the M-N-C active sites, acting as a complemental structure, and this study was later endorsed by others authors [25,32,33]. Here, it is emphasized that the M-N-C species may, eventually, not only be formed on pure carbon powders, but also on the shell of the encapsulated metal nanoparticle structures, and this is an additional difficulty for the correct determination of the activities of these different compounds that are formed during the pyrolysis step.

However, most of the studies in literature lack of a systematic investigation for the comparison of the activities of the different compounds produced in parallel during the pyrolysis step for obtaining M-N-C structures. Hence, in this study, in order to further advance in the knowledge of which structure is more active for the ORR, different electrocatalysts, formed by different compounds and/or by different structures, were selectively synthesized. Intentionally, to compare the activities, bimetallic FeCo-N-C, with an excess of metals, were synthesized to induce the formation of encapsulated metal nanoparticle in addition to the nitrogen-coordinated Fe and Co species. The materials were characterized, and their electrocatalytic activity of the ORR in acid and alkaline media are presented in the text, arranged in order of increasing the structural complexity of the electrocatalysts.

2. Experimental details

2.1. Reactants and materials

$Fe(NO_3)_3.9H_2O$, $Co(NO_3)_2.6H_2O$, $C_3H_4N_2$, C_2H_5OH, C_3H_7OH, KOH, H_2SO_4, were acquired commercially from Sigma-Aldrich. Vulcan carbon XC-72R was purchased from Cabot Corp.

2.2. Synthesis of the Electrocatalysts

Vulcan carbon, for all synthesized materials, was previously treated at 1050 °C, under argon atmosphere, using a tubular oven (MAITEC). Briefly, the synthesis starts with an impregnation step, in which the components were mixed in 50 mL ethanol solution and left under stirring during 5 h at 60 °C. After the evaporation of the ethanol at 80 °C, the resulting powders were subjected to different heat treatments. For all cases, the mass of the precursor reactants were: iron nitrate 150 mg, cobalt nitrate 98 mg, imidazole 160 mg, and all the materials contains Vulcan carbon (200 mg). The synthesis conditions for all studied materials are summarized in Table 1.

Table 1
Summary of the synthesis conditions used for each studied material.

Sample name	Metal precursors (Fe and Co)	Imidazole	Heat treatment condition
C 1050 Ar	No	No	1050 °C Ar for 1h
FeCo@C	Yes	No	1050 °C Ar for 1h
FeCo@NC*	Yes	No	950 °C NH_3 for 1h
N-C 1050 N_2	No	No	1050 °C N_2 for 1h
N-C 950 NH_3	No	No	950 °C NH_3 for 1h
N-C 700 N_2-Imi	No	Yes	700 °C N_2 for 10h
FeCo-N-C 700 N_2	Yes	No	700 °C N_2 for 10h
FeCo-N-C 950 NH_3	Yes	No	950 °C NH_3 for 1h
FeCo-N-C 1050 N_2	Yes	No	1050 °C N_2 for 1h
FeCo-N-C 1050 N_2-Imi	Yes	Yes	1050 °C N_2 for 1h
FeCo-N-C 700 N_2-Imi	Yes	Yes	700 °C N_2 for 10h

* FeCo@NC was synthesized *via* thermal treatment of FeCo@C in NH_3 atmosphere.

Based on all compounds that can be produced during the pyrolysis step in the synthesis of M-N-C electrocatalysts, the materials herein studied were divided into four groups: Group I: carbon and carbon-encapsulated iron-cobalt nanoparticles (in the other words, insertion of metal onto carbon matrices), represented hereafter as C 1050 Ar and FeCo@C, respectively; Group II: Nitrogen-doped carbon and nitrogen-doped carbon-encapsulated iron-cobalt nanoparticles, represented by N—C and FeCo@NC, respectively; Group III: nitrogen insertion on a metal-carbon matrices with N_2 or NH_3 as nitrogen precursor, represented by FeCo-N-C 700 or 1050 N_2 and FeCo-N-C 950 NH_3 and; Group IV: nitrogen insertion on a metal-carbon matrix with imidazole as nitrogen precursor, represented by FeCo-N-C 700 N_2-Imi or 1050 N_2-Imi.

2.3. Electrocatalyst characterization

The crystalline structures of the metallic species were determined by X-ray diffraction (XRD) using a RIGAKU diffractometer model ULTIMA IV (RIGAKU, Tokyo, Japan) equipped with Cu Kα (λ = 0.154 nm) as the radiation source. The diffractograms were obtained in the reflection mode, in the range of 10 to 100° (2θ), with a scan rate of 1.0°/min, and with a step size of 0.03°. The samples were analyzed using the standard crystal data sheets of the EVA program (Brucker). Transmission Electron Microscopy (TEM) measurements were performed in a JEOL JEM 2100 F microscopy (operated at 200 kV). The samples for TEM were prepared by dispersing the powders in isopropyl alcohol under an ultrasonic bath, for 10 min, and a 3.0 μL aliquot was pipetted onto a copper grid (3.0 mm in diameter and 300 mesh) covered by carbon fibers, followed by drying in a desiccator, under vacuum, for 12 h. Structural analyses were also investigated by X-ray Absorption Spectroscopy (XAS) in the X-ray absorption near edge structure (XANES) and X-ray Absorption Fine Structure (EXAFS) regions, at the Fe (7112 eV) and Co (7709 eV) K edges. The XAS measurements were performed in the XAFS-2 beamline, at the Brazilian Synchrotron Light Laboratory (LNLS). The XAS samples were formed by pressing Nafion®-agglutinated electrocatalyst powders (30 wt%. of Nafion) with 1.0 ton of pressure, forming rectangular pellets. The signals were analyzed using the Athena software. The EXAFS oscillations were adjusted by standard procedures in R space using K^3 weight Fourier transform.

2.4. Electrochemical experiments

The experiments for the ORR electrocatalysis were conducted in a conventional three electrodes electrochemical cell. A ring-shaped gold foil was utilized as a counter electrode, and an Ag/AgCl (KCl sat.) was used as a reference electrode. All potentials were converted to the Reversible Hydrogen Electrode (RHE) scale. The working electrodes were composed by the electrocatalysts deposited as a thin layer over a glassy carbon disk, 5.0 mm diameter (0.196 cm^2), of a rotating disk electrode, RDE (Pine Inst.). The electrocatalytic layers were prepared by depositing 25 µL aliquots of the powder suspensions (inks) onto the glassy carbon disks of the RDE (previously polished in alumina, 0.5 µm). The inks were prepared from 5.0 mg of the electrocatalyst and 50 µL of a Nafion solution (5.0 wt.%) in 1.0 mL isopropanol. The Pt/C (20 wt.%, E-TEK) electrode, used for comparison, was prepared from 3.0 mg of the electrocatalyst and 50 µL of a Nafion solution (5.0 wt.%) in 1.0 mL isopropanol, pippeting a 10 µL aliquot onto RDE glassy carbon disk. The experiments were conducted in 0.5 mol L^{-1} H_2SO_4 and/or in 1.0 mol L^{-1} KOH. The electrolytes were prepared using ultrapure water obtained in a Milli-Q system (Millipore). The experiments for ORR were obtained by means of steady-state polarization curves at 5.0 mV s^{-1}, with O_2-saturated electrolyte, at a rotation speed of 1600 rpm. All measurements were conducted at 25 °C using an AUTOLAB (PGSTAT30) potentiostat.

3. Results and discussion

To better analyze the electrocatalyst structural features that govern the ORR activity, the results were arranged following the order of increasing the structural complexity of each material. In all figures hereafter shown, the ORR polarization curves obtained for C 1050 Ar were maintained for comparison purposes, as it is the least active material in both electrolytes. Fig. 1(A) presents the XRD spectrum for the carbon-encapsulated iron-cobalt nanoparticles, FeCo@C (modification of carbon by the insertion of metal atoms). It is clearly seen the presence of three different phases: amorphous carbon, as evidenced by the peak at 2θ = 25°, Fe_3Co_7 alloy (intermetallic), manifested by the peaks at 2θ *ca.* 43, 65 and 82°, and Fe and Co non-stoichiometric carbides (FeC_x and CoC_x), identified by the peaks at *ca.* 42, 51, and 76°. The TEM image for this material (Fig. 1(B)) shows the presence of nanoparticles (dark cores) encased by thick carbon layers (indicated by the inserted black arrows), this being clearly seen in the zoom in of an individual nanoparticle in the figure inset. It is noted that the nanoparticles are fully encapsulated by carbon layers, and these two phases are completely attached by each other (total "adhesion", with no gap between the metal nanoparticle and the carbon layer). As already mentioned in the literature, this is due to the lattice parameters compatibility of the metal or the metal carbide, and of the graphitic carbon layers [14,30,34–36]. The formation of carbon-encapsulated metal nanoparticles can be explained by a graphitization process, catalyzed by metallic iron and/or metallic cobalt atoms at high temperatures [30]. One can also note some non-encapsulated nanoparticles in the TEM image of Fig. 1(B). However, for all cases, as the electrodes were first submitted to cyclic voltammetry in H_2SO_4 electrolyte, prior the ORR polarization curves, all remaining, non-encapsulated nanoparticles undergo dissolution, and, therefore, they do not influence in the overall ORR activity. Fig. 1(C) and (D) show the polarization curves obtained for the ORR in acid and in alkaline electrolyte, respectively, for the C 1050 Ar and FeCo@C electrocatalysts. As can be observed, the overpotentials for the ORR of both materials are lower in alkaline electrolyte, evidencing that carbon is more active in alkaline media than acid media, probably due to the so-called “kinetic facility” in alkaline media, as suggested by Mukerjee [37]. Also, it is seen that there is no increase in electrocatalytic activity when the metals are added to the carbon structure (metal nanoparticles and/or metal carbides encapsulated by carbon) forming the core-shell architectures, both presenting onset potentials of *ca.* 0.22 and 0.84 V in acid and in alkaline media, respectively. Here, one cannot exclude some metal-induced electronic modification on the carbon shell layer as a result of the interaction between the metal core and the carbon shell. Nevertheless, this may be valid only when the shell layer is very thin, as observed in previously published studies in the literature [14], and, so, this is not the case in

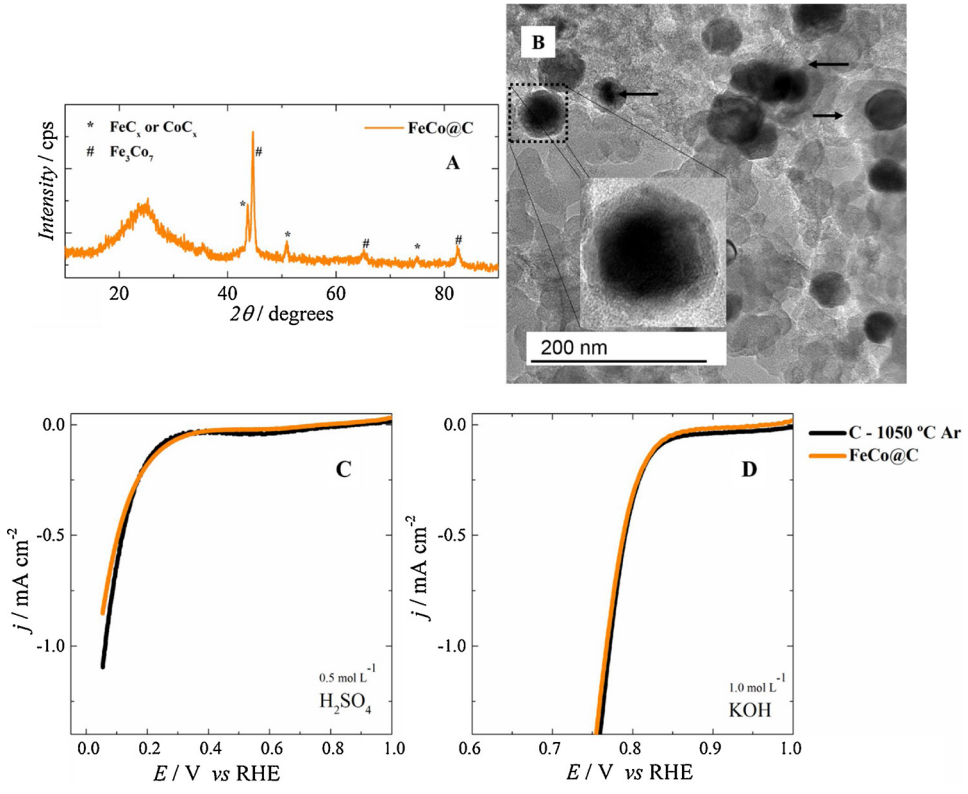

Fig. 1. X-ray powder diffraction (A), transmission electron microscopy image (B), and steady-state polarization curves, at high potential domain, in O_2-saturated 0.5 mol L^{-1} H_2SO_4 (C) and in 1.0 mol L^{-1} KOH electrolyte (D), for the FeCo@C electrocatalyst (carbon-encapsulated metal nanoparticles) of the Group I. Scan rate of 5.0 mV s^{-1} and rotation rate of 1600 rpm. The curve obtained for C 1050 Ar was included for comparison.

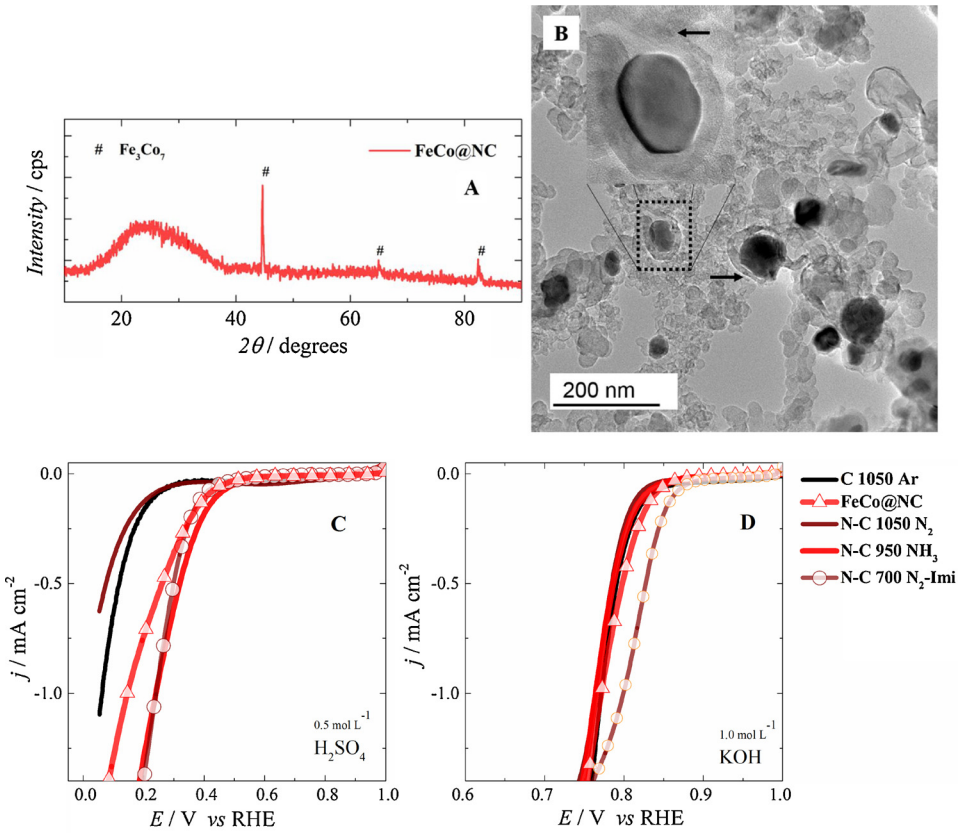

Fig. 2. X-ray powder diffraction (A) and transmission electron microscopy image (B) for the FeCo@NC material, and steady-state polarization curves, at a high potential domain, in O_2-saturated 0.5 mol L^{-1} H_2SO_4 (C) and in 1.0 mol L^{-1} KOH (D) electrolyte, for all electrocatalysts of Group II (nitrogen-doped carbon and nitrogen-doped carbon-encapsulated metal nanoparticles). Scan rate of 5.0 mV s^{-1} and rotation rate of 1600 rpm.

the present study.

The effect of introducing nitrogen (N-doping) on carbon and on carbon-encapsulated iron-cobalt nanoparticles are presented below. The XRD spectra obtained for the carbon materials submitted to the thermal treatment in N_2 or NH_3 and that for carbon modified with the impregnation of imidazole, followed by pyrolysis in N_2, are presented in Figure S1. It is noted that the addition of nitrogen does not produce any change in the XRD spectra for all materials, since nitrogen may only dope the carbon structure and, therefore, do not forming any crystalline phase. In fact, all samples show the two peaks at *ca.* 25° and 44°, ascribed to the (002) carbon reflection planes.

The XRD for FeCo@C treated in NH_3 atmosphere at 950 °C (FeCo@NC), presented in Fig. 2 (A), shows peaks related to the Fe_3Co_7 alloy phase, as also observed for the initial material (FeCo@C). The iron and cobalt atoms initially presented as metal carbides on FeCo@C might now be converted to metal alloy phase due to the chemical reaction with NH_3 atmosphere (which is a reducing atmosphere). The TEM image for FeCo@NC, shown in Fig. 2(B), clear evidence that the metallic nanoparticles remain in the material, but it is worth to note that the graphitic shell layer is now detached from the nanoparticle surface (depicted by the inset arrows). This aspect is ascribed to the lattice mismatch between the metal nitride phase on the surface of the metal core and the N-doped carbon shell, produced after the reaction between iron, cobalt and carbon atoms with NH_3. Nevertheless, the amount of the metal nitride phase is too low when compared to that of the alloy phase and, so, the XRD peaks from this phase cannot be clearly evidenced in the spectrum.

The ORR polarization curves, presented in Fig. 2(C) and (D), show that, when nitrogen is inserted in pure carbon powder by using thermal treatment in N_2 atmosphere at 1050 °C (N-C 1050 N_2), it does not result in an increase in the ORR activity in both electrolytes. This may indicate that there is no nitrogen insertion or that the extent of the nitrogen insertion was not enough to produce an observable change in the ORR polarization curve. Nevertheless, when the source of nitrogen is changed NH_3, at 950 °C, the resulting material (N-C 950 NH_3) presents an increase in the ORR onset potential to 0.4 V in the acidic electrolyte. This was also the case of the material formed by carbon-encapsulated iron-cobalt nanoparticles treated in NH_3 (FeCo@NC), reaching the same onset potential.

These curves strongly evidence that the insertion of the nitrogen atoms into the carbon structure produces active sites for the ORR. If so, it is indirectly concluded that, if N_2 is the nitrogen source, the thermal treatment at 1050 °C is not high enough for adding nitrogen into the carbon structure, when pure carbon is submitted to this treatment. On the other hand, NH_3, which is much more reactive than N_2, can add nitrogen to the carbon structure, even at lower temperatures (950 °C for example). As can be noted in Fig. 2(C) and (D), the N-doping on carbon *via* reactive gas is significant for the ORR in acid media, but it presents a negligible change on the ORR polarization curve in the alkaline electrolyte. Conversely, this scenario appears to be different when the nitrogen insertion in the carbon matrix is made by using a nitrogen-enriched molecule, such as imidazole, at the beginning of the synthesis (impregnation step). In this synthesis, low-temperature pyrolysis (700 °C) in N_2, was used instead of the NH_3 atmosphere in order to investigate the role of the nitrogen incorporation coming uniquely from the imidazole. As mentioned above, temperatures equal or below 1050 °C are not high enough to incorporate nitrogen onto the carbon matrix using N_2 as the source. According to the ORR polarization curves shown in Fig. 2(C) and (D), the N-C 700 N_2-Imi material (N-doping *via* nitrogen-rich molecule) showed an increase in electrocatalytic activity in both media in relation to that of pure carbon, with the onset potentials being raised to 0.4 and 0.86 V, respectively. So, since pure carbon is already active in alkaline electrolyte due to the facilitated kinetics [37], only a high level of N-doping (obtained by using imidazole) is able to induce a significant shift of the ORR half-wave potential to higher values in alkaline media. The superficial impregnation of the carbon powder by imidazole, followed by the pyrolysis procedure, may result in a carbon nanostructure with a superficial nitrogen-rich

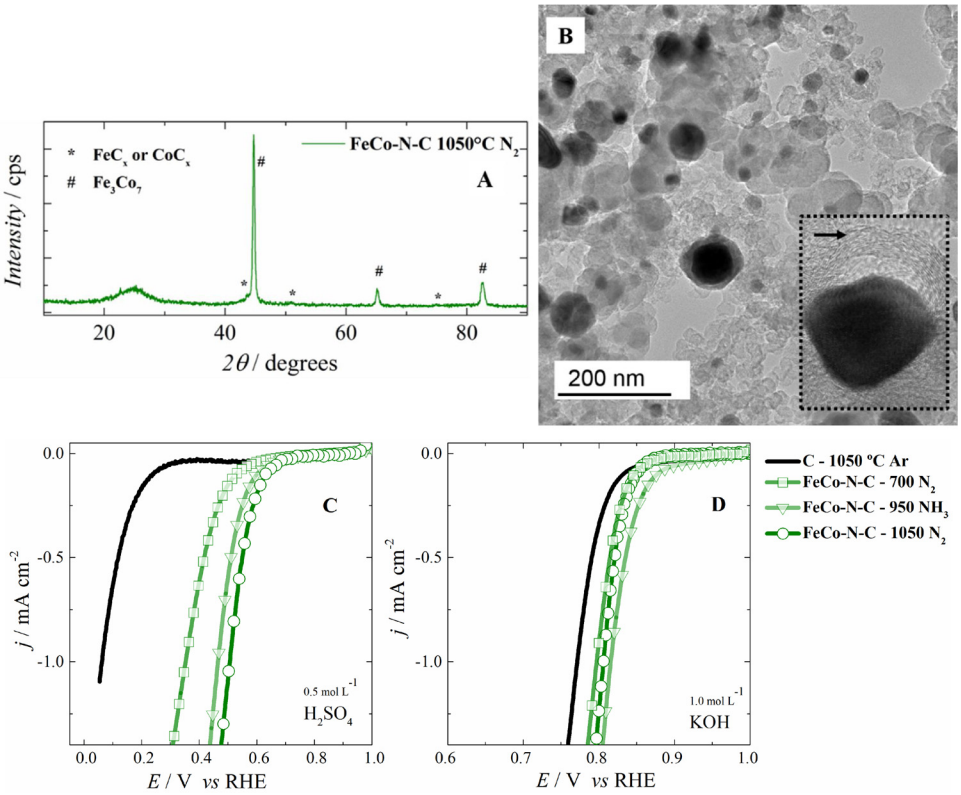

Fig. 3. X-ray powder diffraction (A) and transmission electron microscopy image (B) for the FeCo-N-C 1050 N_2 material, and steady-state polarization curves, at a high potential domain, in O_2-saturated 0.5 mol L^{-1} H_2SO_4 (C) and in 1.0 mol L^{-1} KOH (D) electrolyte, for all electrocatalysts of Group III (presence of metal, carbon and nitrogen, for which nitrogen is provided by the N_2 or NH_3 atmosphere). Scan rate of 5.0 mV s^{-1} and rotation rate of 1600 rpm.

graphitic carbon layer. This may arise from the high nitrogen-to-carbon atomic ratio of the imidazole molecule (2:3), and it may explain the higher ORR activity encountered for the N-C 700 N_2-Imi material in alkaline electrolytes. Probably, the enhanced ORR activity of the N-doped carbon in relation to that of pure carbon is a consequence of the carbon polarization induced by the neighboring nitrogen atoms due to their higher electronegativity, resulting in positively charged carbon atoms. This may facilitate the stabilization of ORR reaction intermediates, enhancing the material's activity for the ORR [34].

It is worth to mention, here, that the lattice mismatch observed in the TEM image for the FeCo@NC is relevant only to prove that some nitrogen atoms were indeed incorporated on the carbon shell, and on the surface of the metal core. The presence or absence of lattice mismatch in these core-shell structures (*i.e.* presence or absence of space (or gap) between the core and the shell) may not have any influence on the material's activity for the ORR. Specific studies should be carried out to clarify this aspect, but this is out of the objective of the present work.

The XRD and TEM image for FeCo-N-C 1050 °C N_2 are presented in Figs. 3(A) and (B), and those for FeCo-N-C 700 °C N_2 and FeCo-N-C 950 °C NH_3 are presented in Figures S2 and S3, respectively (Group III - pyrolysis of iron, cobalt and carbon precursors, in N_2 or NH_3 atmosphere). The TEM images show similar morphological aspects as observed for the Group I, with the formation of carbon-encapsulated metal nanoparticles, and the occurrence of graphitic layers. Also, here, the graphitic carbon layers are detached from the metal nanoparticles surface (indicated by the black arrow inserted), for those materials treated in N_2 at 1050 °C or in NH_3. As mentioned above, this is due to the lattice mismatch of the metal or metal nitride and the N-doped carbon layer that is produced during the thermal treatment, likewise indicating that some nitrogen atoms were inserted into the material's structure. According to the XRD profiles, the material treated in the N_2 atmosphere produced metallic alloy (Fe_3Co_7), and metal carbide phases, but only the material treated at 1050 °C was able to produce N-doped carbon shells. As the XRD result for FeCo-N-C 700 N_2 (Figure S2) does not evidence the formation of metal nitride, and the TEM image shows some nanoparticles with the detached graphitic shell, the lattice mismatch may arise from the formation of a shell with a high nitrogen-doping level. Interestingly, this high nitrogen doping level was not evidenced when pure carbon powder was treated in N_2 at 1050 °C. So, for FeCo-N-C 1050 N_2 the increase in the nitrogen doping level may be ascribed to the beneficial effect of iron and/or cobalt; the metal/carbon atoms may, somehow, catalyze the nitrogen insertion. Therefore, as also discussed below, the materials of Group III might contain M-N-C species even in the shell of the encapsulated nanoparticles. For the material treated in NH_3, the lattice mismatch is due to the metal nitride formation (M_xN_y phase, with M = Fe or Co), probably located on the surface of the nanoparticles located in the core, as evidenced by the XRD result presented in Figure S3(A). Note, here, that these metal nitrides do not contribute to the ORR activity, because they do not remain in the material after the voltammetric cycles in the acidic media (undergo dissolution) [38].

One can also observe a considerable improvement of the activity for the ORR for the materials of Group III. Interestingly, higher shifts were observed in the ORR onset potentials for the materials treated in N_2 at 1050 °C and in NH_3, for which their TEM images indirectly show the higher level of N-doping (discernible lattice mismatch). In the acidic electrolyte, their onset potentials were at the interval between 0.5 - 0.6 V, which is an important improvement in their activities when compared to those of the materials of Group II. In the alkaline electrolyte, the materials of Group III experienced an enhancement to *ca.* 0.86 V, against 0.80 V for those of Group II (with exception of the imidazole-treated material, which showed an increased ORR activity, with an onset potential of 0.85 V).

The obtained results for the morphological characterization of the electrocatalyst synthesized using imidazole as the nitrogen source (Group IV) are presented in Figs. 4(A) and (B). One can observe that the obtained XRD spectra are similar to those of Group III. The material treated in N_2 at 700 °C presents iron-cobalt alloy phases, and the material treated in N_2 at 1050 °C (Figure S4) presents metal carbide, in

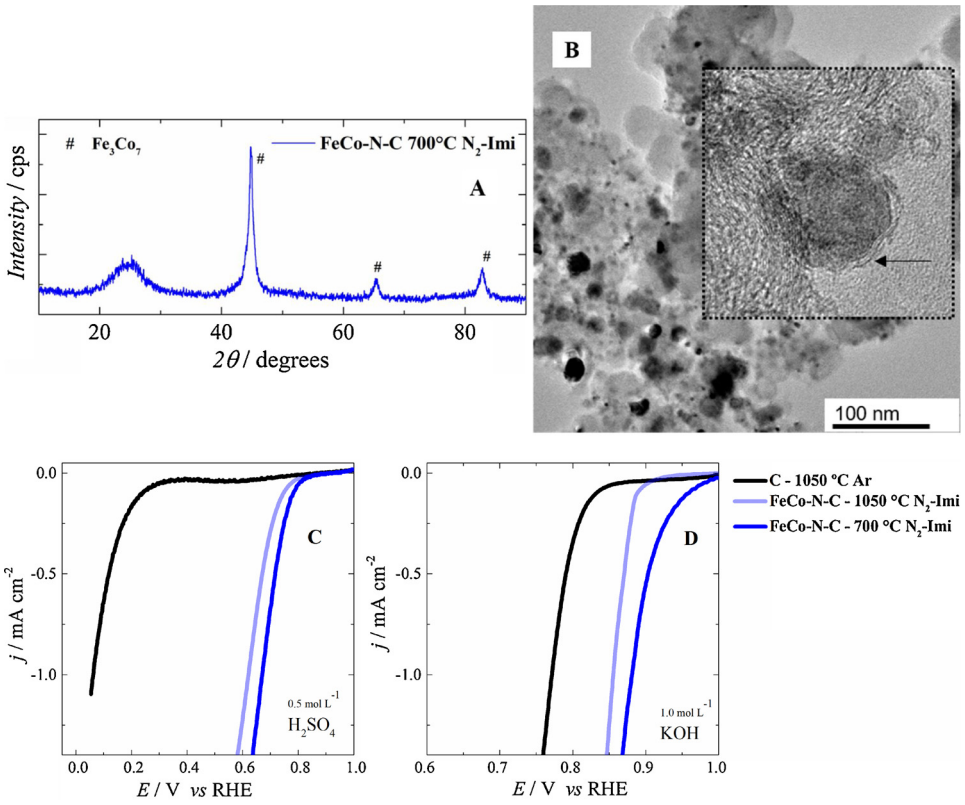

Fig. 4. X-ray powder diffraction (A) and Transmission electron microscopy image (B) for the FeCo-N-C 700 N_2 Imi material, and steady-state polarization curves, at a high potential domain, in O_2-saturated 0.5 mol L^{-1} H_2SO_4 (C) and in 1.0 mol L^{-1} KOH (D) electrolyte for all electrocatalysts of Group IV (presence of metal, carbon and nitrogen, for which nitrogen is provided by the imidazole molecule). Scan rate of 5.0 mV s^{-1} and rotation rate of 1600 rpm.

addition to an iron-cobalt alloy phase. The TEM for FeCo-N-C 1050 N_2-Imi (Fig. S4 (B)) shows only a slight detachment of the carbon shell, but for FeCo-N-C 700 N_2-Imi the image shows a complete adhesion of this graphitic carbon shell (Fig. 4(B)), evidencing the non-formation of metal nitrides at 700 °C. The ORR polarization curves for FeCo-N-C 700 N_2-Imi and FeCo-N-C 1050 N_2-Imi, presented in Fig. 4(C) and (D), clearly show the highest shift of the ORR onset potential among all studied electrocatalysts, reaching 0.75 and 0.78 V in acid media, and 0.89 and 0.95 V in alkaline media, respectively.

In order to obtain further insights into the electrocatalyst structure - ORR activity correlation, XANES, and EXAFS spectra, at the Fe and Co K edges, were obtained for some selected materials (FeCo@C 1050 Ar, FeCo-N-C 1050 N_2, and FeCo-N-C 700 N_2 Imi). The XANES spectra, obtained at the Fe and Co K edges, for all studied materials (Fig. 5(A) and (C)), show profiles that are not very similar to the reference iron foil (bulk Fe). This may arise from the different electronic structures of the metals in the electrocatalyst samples, that are mostly present as nanoparticles, and the bulk metals in the reference foil. However, important structural features can be obtained analyzing the Fourier Transform (FT) of the EXAFS oscillations at the Fe and Co K edges, presented in Fig. 5(B) and (D), respectively. One can note that the FT for FeCo@C electrocatalyst has a large peak centered at *ca.* 2.1 Å for both edges. This is related to the Fe-Fe and Co-Co first coordination shell of metallic phases, which comes from the carbon-encapsulated metal nanoparticles in the sample. Nevertheless, for the materials of the Groups III and IV (FeCo-N-C 1050 N_2, and FeCo-N-C 700 N_2-Imi), it is observed that this peak is accompanied by a "shoulder" centered at *ca.* 1.5 Å. This is ascribed to the bond of Fe or Co with atoms with low atomic numbers, such as N or O (most likely to be N in the present case). So, despite most of the signal comes from the metallic species (encapsulated Fe-Co nanoparticles), these results evidence that part of the iron and cobalt atoms in the sample are involved in the Fe-N and Co-N bonds, revealing the presence of M-N-C species (nitrogen-coordinated iron and cobalt inserted in the carbon matrix). Here, it is worth to note that the main FT peak obtained for the measurements at the Co K edge (Fig. 5(D)), for the FeCo@C and FeCo-N-C 1050 N_2 samples, instead of appearing at 2 Å (Co-Co coordination from metallic cobalt), it is slight shifted to 2.1 Å. This peak is an indicative of the presence of cobalt carbide. This corroborates with the XRD results presented in Figs. 1 and 3, explaining that most of Co atoms are likely present in the carbide phase (encapsulated by carbon), rather than as a metallic nanoparticle encapsulated by carbon, for these two samples. The carbide phase, however, has no activity for the ORR, since the ORR polarization curve for the FeCo@C material does not show any improvement in activity in relation to that of pure carbon (Fig. 1(C) and (D)).

A brief scheme compiling the ORR curves in their respective groups is exposed in Fig. 6. The materials were grouped based on their structure/composition and ORR activity: Group I - black and orange colors; materials with basal ORR activity, such as carbon and metal-carbon matrix; Group II - red and wine colors: materials poorly active towards the ORR, with the insertion of nitrogen (N-doping) in carbon matrix; Group III – green colors: materials with intermediate activity for the ORR, with metal, nitrogen, and carbon, for which the nitrogen atom is originated from the N_2 or NH_3 atmosphere; and Group IV – blue colors: materials with high activity for the ORR, with metal, nitrogen carbon matrices, but now nitrogen is originated from a nitrogen-rich molecule (imidazole). Here, it is emphasized that the medium and high electrocatalytic activity for ORR is achieved only for the materials that possess M-N-C species in their composition (see EXAFS results). Indeed, the ORR activities for the FeCo-N-C 700 N_2-Imi electrocatalyst, in both H_2SO_4 and KOH electrolytes, approach that of the state-of-the-art carbon-supported platinum nanoparticles (Pt/C), as can be seen in the steady-state polarization curves presented in Fig. 5S.

The sequence of these curves, presented the scheme of Fig. 6, illustrates a behavior that was not yet clearly described or concluded in the literature to date, especially for both types of electrolytes (acid and alkaline), and some statements can be drawn, as follows: (i) carbon-encapsulated metal nanoparticles do not have higher activity higher than pure carbon (Vulcan); (ii) N-doped carbon or N-doped carbon-

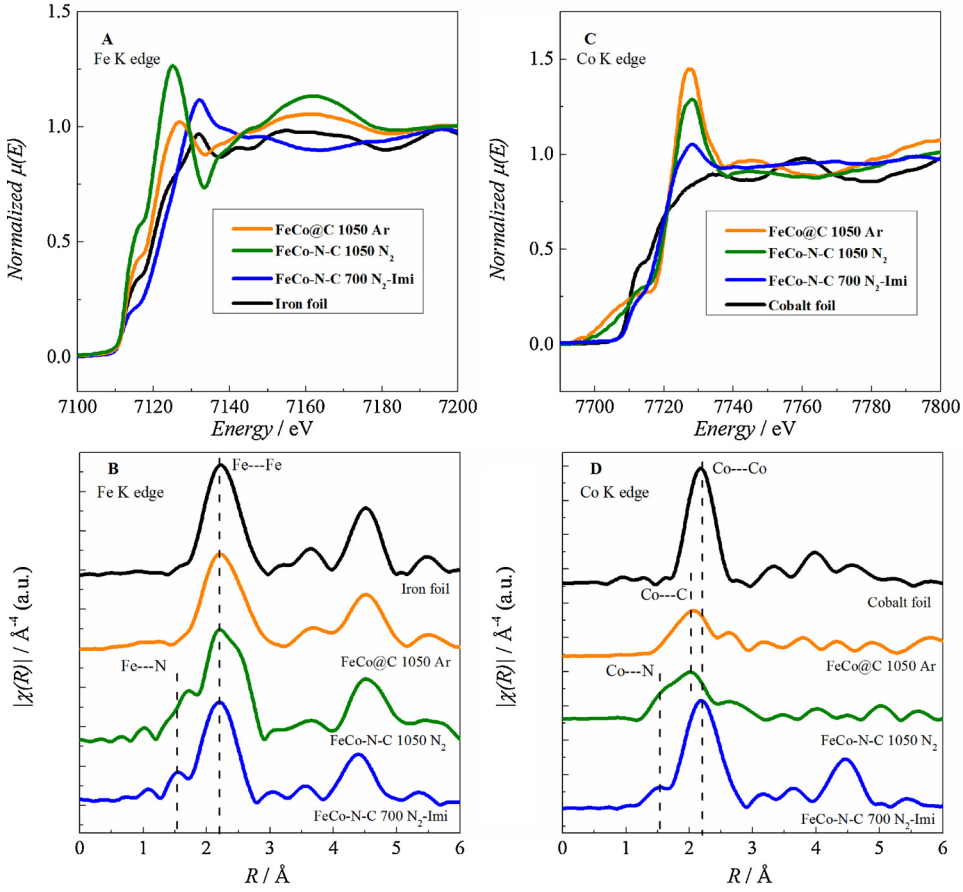

Fig. 5. XANES (A) and (C) and Fourier Transform of the EXAFS oscillations, K^3-weighted, (B) and (D), at the Fe (7112 eV) and Co (7709 eV) K edges for some selected electrocatalysts, as indicated in the figure insets. The spectra obtained for bulk iron and cobalt (metallic foils) were included for comparison.

encapsulated metal nanoparticle, FeCo@NC (nitrogen insertion only in the graphitic shell), show an increased ORR activity when compared to that pure carbon, and their activities are dependent on the nitrogen doping level, and; (iii) The inclusion of a nitrogen-rich molecule, such as imidazole, during the initial step of the synthesis, produced an electrocatalyst with high ORR activity [39]. According to the EXAFS data, this strategy generated Fe-N and Co-N bonds; *i.e.*, it allowed the formation of M-N-C species.

The fact that the addition of a nitrogen-rich molecule resulted in the material with the highest activity for the ORR can be attributed to two main effects: (i) the partial complexation of the metal ions by imidazole, allowing better dispersion of the metal species on the carbon

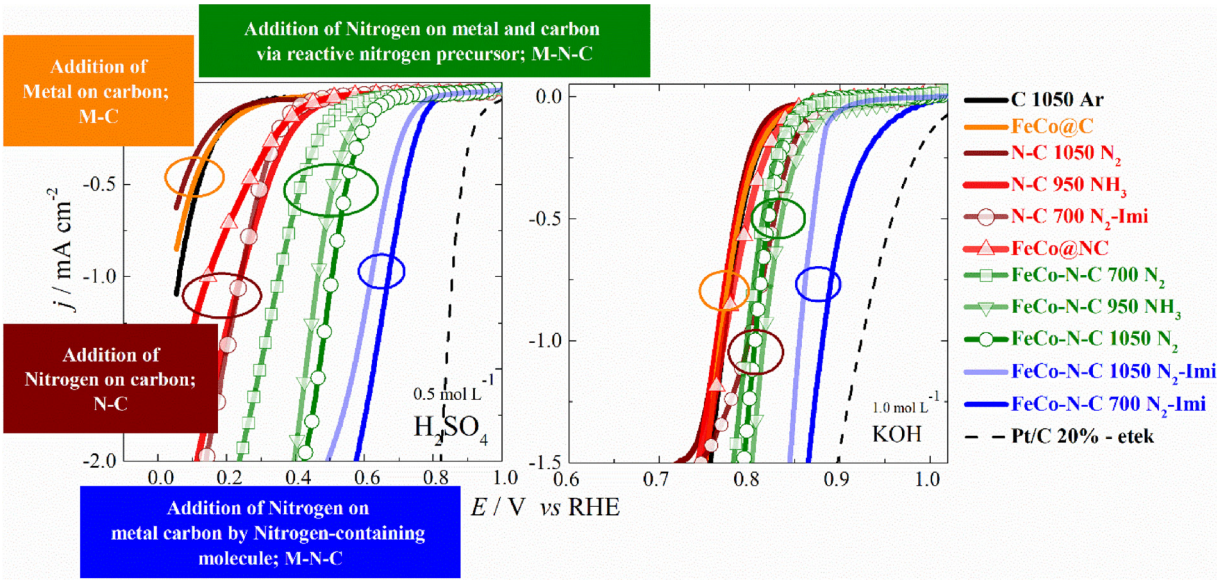

Fig. 6. Scheme compiling the ORR steady-state polarization curves into four different groups, as indicated in the figure insets. The curves obtained for state-of-the-art carbon-supported platinum nanoparticle (Pt/C) were included for comparison. Scan rate of 5.0 mV s^{-1} and rotation rate of 1600 rpm.

powder surface [40], and; (ii) the increased N-doping level due to the high availability of nitrogen in the imidazole molecule, as also indicated a previous studies [41,42]. By using the impregnation of imidazole on the carbon surface, the surface of the resulting powder may have a high-density of nitrogen atoms (imidazole has a nitrogen to carbon ratio of 2–3) and, so, upon annealing, these nitrogen atoms are available, and may be incorporated into the carbon matrix (at least on the superficial layers), as indicated by the results shown here. When iron and/or cobalt precursors are impregnated together with imidazole, the formation of the M-N-C species, after the pyrolysis step, would be facilitated due to the proximity of the metals and the nitrogen atoms, producing an electrocatalyst with high activity [2,40].

The conclusion stating that the M-N-C species has high ORR activity is not surprising, since this active site mimics natural catalysts, such as cytochrome *c*, and it has also been identified in previous studies [2,6,24]. However, it is worth to note that identifying the individual activity contributions from the all other compounds generated during the synthesis of this class of material *via* pyrolysis is a complex, and a difficult task to be accomplished. As can be noted in the TEM images, all materials that were synthesized with iron and cobalt precursors generated carbon or N-doped carbon-encapsulated nanoparticles. For example, FeCo-N-C 700 N_2-Imi and FeCo-N-C 1050 N_2-Imi possess both, N-doped carbon-encapsulated Fe-Co nanoparticles, and FeCo-N-C species (coordinated structure; Fe-N and Co-N bonds). However, even being present at a low extent, the last structure is the one that is responsible for the high ORR onset potentials encountered for these materials. As these materials are mostly formed by the encapsulated structures, this may conduct to a misleading conclusion that such structure is highly active for the ORR (note that FeCo@C and FeCo@NC have low ORR onset potentials). As noted in Fig. 6, different electrocatalytic activities can be obtained by controlling the composition and/or the thermal treatment atmosphere and temperature. It is observed that FeCo-N-C 700 N_2-Imi presents higher electrocatalytic activity than FeCo-N-C 1050 N_2-Imi. Although the explanation for this last observation is difficult to be delineated, one can consider that the higher temperature of thermal treatment may destroy part of the coordinated structure, and induce the further formation of metal nanoparticles, which have low activity compared to the coordinated structures. As a matter of fact, the central aim of this work was to identify, among the different kind of structures that are formed in parallel to M-N-C (carbides, encapsulated metal nanoparticles, etc), if some of them have high electrocatalytic activity for the ORR. Based on the evidence presented above, it can be affirmed that carbon-encapsulated metal nanoparticles or even nitrogen-doped carbon-encapsulated metal nanoparticle cannot be responsible for the high half-wave potentials encountered in polarization curves for the ORR electrocatalysts formed by metal, nitrogen, and carbon. The results presented herein salient that only the M-N-C species is responsible for the high half-wave potentials for the ORR whether in acid or alkaline electrolytes. No attempt, however, was focused in the present investigation to the optimization of the synthesis conditions. This will be conducted in a next study. Nonetheless, this work contributes to open a roadway for the rational design of M-N-C type electrocatalysts. Accordingly, the synthesis of M-N-C electrocatalysts should be focused on the use of nitrogen-rich molecules that are able to strongly complex the metal atoms during the impregnation step, and on carbon powders with the high surface area, to allow higher dispersion of the metal atoms on their surfaces.

4. Conclusions

Different metal-nitrogen-carbon electrocatalysts were synthesized by regular pyrolysis procedures and arranged, step-by-step, in an order of increasing their structural complexity. Carbon-encapsulated iron-cobalt nanoparticles do not present significant ORR activity, showing the same onset potential of pure carbon. The insertion of nitrogen on carbon or on the carbon of carbon-encapsulated iron-cobalt material, *via* thermal treatment in N_2 or NH_3 atmosphere, or using a nitrogen-rich molecule, resulted in materials that present an increase in the ORR activity when compared to that of pure carbon. This fact evidences that N-doped carbon is, indeed, an active site for the ORR. When the precursors of carbon (Vulcan), nitrogen (N_2, NH_3 or imidazole) and iron and cobalt (metal nitrates) were present in the synthesis, the resulting electrocatalyst showed a pronounced enhancement in the ORR activity. However, only the introduction of a nitrogen-rich molecule such as imidazole, during the impregnation step, was efficient to produce an electrocatalyst with high half-wave potential for the ORR. This was ascribed to two main effects: (i) the partial complexation of the metal ions by imidazole, allowing better dispersion of the metal atoms on the carbon powder surface, and; (ii) the increased N-doping level due to the high availability of nitrogen in the imidazole molecule. The FeCo-N-C 700 N_2-Imi electrocatalyst presented the highest activity towards the ORR and, according to the EXAFS results, this seems to be correlated to the more efficient formation of metal atoms coordinated by nitrogen, inserted in the graphitic matrix (M-N-C). Finally, and most important, only when M-N-C species (coordinated structure) are present in the material, even at low quantities, the ORR polarization curves display high values of half-wave potentials. Carbon-encapsulated metal nanoparticles or even nitrogen-doped carbon-encapsulated metal nanoparticles, that are, eventually, components of the M-N-C electrocatalysts cannot be responsible for the high ORR half-wave potentials since the polarization curves of the individual components evidence low ORR activities.

Acknowledgments

Authors gratefully acknowledge financial support from FAPESP (Fundação de Amparo à Pesquisa do Estado de São Paulo, F.H.B.L. grant No. 2016/13323-0 and 2013/16930-7 and N.A.G. grant No. 2016/06197-9), CNPq (Conselho Nacional de Desenvolvimento Científico e Tecnológico, F.H.B.L. grant No. 306469/2016-2), CAPES (Coordenação de Aperfeiçoamento de Pessoal de Nível Superior, F.E.R.O. grant No.1255731), and the Brazilian Synchrotron Light Laboratory (LNLS, XAFS2 beamline) for assisting with the XAS experiments. The authors thank the technician Gabriel Christiano da Silva by his support in the TEM images acquirement.

Appendix A. Supplementary data

Supplementary material related to this article can be found, in the online version, at doi:https://doi.org/10.1016/j.apcatb.2019.04.057.

References

[1] K. Mamtani, D. Singh, J. Tian, J.-M.M.M. Millet, J.T. Miller, A.C. Co, U.S. Ozkan, Evolution of N-Coordinated Iron–carbon (FeNC) catalysts and their oxygen reduction (ORR) performance in acidic media at various stages of catalyst synthesis: an attempt at benchmarking, Catal. Lett. 146 (2016) 1749–1770, https://doi.org/10.1007/s10562-016-1800-z.

[2] A.A. Gewirth, J.A. Varnell, A.M. Diascro, Nonprecious metal catalysts for oxygen reduction in heterogeneous aqueous systems, Chem. Rev. 118 (2018) 2313–2339, https://doi.org/10.1021/acs.chemrev.7b00335.

[3] A. Kongkanand, M.F. Mathias, The priority and challenge of high-power performance of low-platinum proton-exchange membrane fuel cells, J. Phys. Chem. Lett. 7 (2016) 1127–1137, https://doi.org/10.1021/acs.jpclett.6b00216.

[4] L. Dubau, L. Castanheira, F. Maillard, M. Chatenet, O. Lottin, G. Maranzana, J. Dillet, A. Lamibrac, J.C. Perrin, E. Moukheiber, A. Elkaddouri, G. De Moor, C. Bas, L. Flandin, N. Caqué, A review of PEM fuel cell durability: materials degradation, local heterogeneities of aging and possible mitigation strategies, Wiley Interdiscip, Rev. Energy Environ. 3 (2014) 540–560, https://doi.org/10.1002/wene.113.

[5] S.D. Knights, K.M. Colbow, J. St-Pierre, D.P. Wilkinson, Aging mechanisms and lifetime of PEFC and DMFC, J. Power Sources 127 (2004) 127–134, https://doi.org/10.1016/j.jpowsour.2003.09.033.

[6] M.L. Pegis, C.F. Wise, D.J. Martin, J.M. Mayer, Oxygen reduction by homogeneous molecular catalysts and electrocatalysts, Chem. Rev. 118 (2018) 2340–2391, https://doi.org/10.1021/acs.chemrev.7b00542.

[7] F. Roncaroli, E.S. Dal Molin, F.A. Viva, M.M. Bruno, E.B. Halac, Cobalt and iron

complexes with N-heterocyclic ligands as pyrolysis precursors for oxygen reduction catalysts, Electrochim. Acta 174 (2015) 66–77, https://doi.org/10.1016/j.electacta.2015.05.136.
[8] R. Jasinski, A new fuel cell cathode catalyst, Nature 201 (1964) 1212–1213, https://doi.org/10.1038/2011212a0.
[9] S. Gupta, D. Tryk, I. Bae, W. Aldred, E. Yeager, Heat-treated polyacrylonitrile-based catalysts for oxygen electroreduction, J. Appl. Electrochem. 19 (1989) 19–27, https://doi.org/10.1007/bf01039385.
[10] H. Jahnke, M. Schönborn, G. Zimmermann, Organic dyestuffs as catalysts for fuel cells, in: F.L. Boschke (Ed.), 61 Top. Curr. Chem. - Phys. Chem. Appl. Dyest. Springer-Verlag Berlin, Heidelberg & New York, 1976, pp. 133–188.
[11] G. Wu, K.L. More, P. Xu, H.-L. Wang, M. Ferrandon, A.J. Kropf, D.J. Myers, S. Ma, C.M. Johnston, P. Zelenay, A carbon-nanotube-supported graphene-rich non-precious metal oxygen reduction catalyst with enhanced performance durability, Chem. Commun. 49 (2013) 3291, , https://doi.org/10.1039/c3cc39121c.
[12] W. Liu, L. Zhang, X. Liu, X. Liu, X. Yang, S. Miao, W. Wang, A. Wang, T. Zhang, Discriminating catalytically active FeN x species of atomically dispersed Fe–N–C catalyst for selective oxidation of the C–H bond, J. Am. Chem. Soc. 139 (2017) 10790–10798, https://doi.org/10.1021/jacs.7b05130.
[13] V. Armel, S. Hindocha, F. Salles, S. Bennett, D. Jones, F. Jaouen, Structural descriptors of zeolitic-lmidazolate frameworks are keys to the activity of Fe-N-C catalysts, J. Am. Chem. Soc. 139 (2017) 453–464, https://doi.org/10.1021/jacs.6b11248.
[14] S.H. Noh, M.H. Seo, J. Kang, T. Okajima, B. Han, T. Ohsaka, Towards a comprehensive understanding of FeCo coated with N-doped carbon as a stable bi-functional catalyst in acidic media, NPG Asia Mater. 8 (2016) e312, https://doi.org/10.1038/am.2016.142.
[15] A. Zitolo, V. Goellner, V. Armel, M.-T. Sougrati, T. Mineva, L. Stievano, E. Fonda, F. Jaouen, Identification of catalytic sites for oxygen reduction in iron- and nitrogen-doped graphene materials, Nat. Mater. 14 (2015) 937–942, https://doi.org/10.1038/nmat4367.
[16] A. Serov, K. Artyushkova, E. Niangar, C. Wang, N. Dale, F. Jaouen, M.-T. Sougrati, Q. Jia, S. Mukerjee, P. Atanassov, Nano-structured non-platinum catalysts for automotive fuel cell application, Nano Energy 16 (2015) 293–300, https://doi.org/10.1016/j.nanoen.2015.07.002.
[17] H.T. Chung, D.A. Cullen, D. Higgins, B.T. Sneed, E.F. Holby, K.L. More, P. Zelenay, Direct atomic-level insight into the active sites of a high-performance PGM-free ORR catalyst, Science 357 (80) (2017) 479–484, https://doi.org/10.1126/science.aan2255.
[18] K. Artyushkova, A. Serov, S. Rojas-Carbonell, P. Atanassov, Chemistry of multitudinous active sites for oxygen reduction reaction in transition metal-nitrogen-carbon electrocatalysts, J. Phys. Chem. C 119 (2015) 25917–25928, https://doi.org/10.1021/acs.jpcc.5b07653.
[19] M. Shao, Q. Chang, J.-P. Dodelet, R. Chenitz, Recent advances in electrocatalysts for oxygen reduction reaction, Chem. Rev. 116 (2016) 3594–3657, https://doi.org/10.1021/acs.chemrev.5b00462.
[20] D. Shin, X. An, M. Choun, J. Lee, Effect of transition metal induced pore structure on oxygen reduction reaction of electro spun fibrous carbon, Catal. Today 260 (2016) 82–88, https://doi.org/10.1016/j.cattod.2015.07.019.
[21] J.Y. Cheon, T. Kim, Y. Choi, H.Y. Jeong, M.G. Kim, Y.J. Sa, J. Kim, Z. Lee, T.-H. Yang, K. Kwon, O. Terasaki, G.-G. Park, R.R. Adzic, S.H. Joo, Ordered mesoporous porphyrinic carbons with very high electrocatalytic activity for the oxygen reduction reaction, Sci. Rep. 3 (2013) 2715, , https://doi.org/10.1038/srep02715.
[22] C. Han, X. Bo, J. Liu, M. Li, M. Zhou, L. Guo, Fe, Co bimetal activated N-doped graphitic carbon layers as noble metal-free electrocatalysts for high-performance oxygen reduction reaction, J. Alloys. Compd. 710 (2017) 57–65, https://doi.org/10.1016/j.jallcom.2017.03.241.
[23] G. Wu, K.L. More, C.M. Johnston, P. Zelenay, High-performance electrocatalysts for oxygen reduction derived from Polyaniline, Iron, and cobalt, Science 332 (2011) 443–447, https://doi.org/10.1126/science.1200832.
[24] J.A. Varnell, E.C.M. Tse, C.E. Schulz, T.T. Fister, R.T. Haasch, J. Timoshenko, A.I. Frenkel, A.A. Gewirth, Identification of carbon-encapsulated iron nanoparticles as active species in non-precious metal oxygen reduction catalysts, Nat. Commun. 7 (2016) 12582, https://doi.org/10.1038/ncomms12582.
[25] M. Sun, D. Davenport, H. Liu, J. Qu, M. Elimelech, J. Li, Highly efficient and sustainable non-precious-metal Fe–N–C electrocatalysts for the oxygen reduction reaction, J. Mater. Chem. A 6 (2018) 2527–2539, https://doi.org/10.1039/C7TA09187G.
[26] C.H. Choi, S.H. Park, S.H. Woo, N-doped carbon prepared by pyrolysis of dicyandiamide with various MeCl2 · xH2O (Me = Co, Fe, and Ni) composites: effect of type and amount of metal seed on oxygen reduction reactions, Appl. Catal. B (2012) 119–120, https://doi.org/10.1016/j.apcatb.2012.02.031.
[27] G. Wu, K. Artyushkova, M. Ferrandon, A.J. Kropf, D. Myers, P. Zelenay, Performance durability of polyaniline-derived non-precious cathode catalysts, ECS Trans. 25 (2009) 1299–1311, https://doi.org/10.1149/1.3210685.
[28] A. Serov, M.H. Robson, M. Smolnik, P. Atanassov, Templated bi-metallic non-PGM catalysts for oxygen reduction, Electrochim. Acta 80 (2012) 213–218, https://doi.org/10.1016/j.electacta.2012.07.008.
[29] J. Wang, Z. Huang, W. Liu, C. Chang, H. Tang, Z. Li, W. Chen, C. Jia, T. Yao, S. Wei, Y. Wu, Y. Li, Design of N-Coordinated dual-metal sites: a stable and active Pt-Free catalyst for acidic oxygen reduction reaction, J. Am. Chem. Soc. 139 (2017) 17281–17284, https://doi.org/10.1021/jacs.7b10385.
[30] K. Strickland, E. Miner, Q. Jia, U. Tylus, N. Ramaswamy, W. Liang, M.-T.T. Sougrati, F.F. Jaouen, S. Mukerjee, Highly active oxygen reduction non-platinum group metal electrocatalyst without direct metal-nitrogen coordination, Nat. Commun. 6 (2015) 1–8, https://doi.org/10.1038/ncomms8343.
[31] U. Tylus, Q. Jia, K. Strickland, N. Ramaswamy, A. Serov, P. Atanassov, S. Mukerjee, Elucidating oxygen reduction active sites in Pyrolyzed Metal–Nitrogen coordinated non-precious-metal electrocatalyst systems, J. Phys. Chem. C 118 (2014) 8999–9008, https://doi.org/10.1021/jp500781v.
[32] W.-J. Jiang, L. Gu, L. Li, Y. Zhang, X. Zhang, L.-J. Zhang, J.-Q. Wang, J.-S. Hu, Z. Wei, L.-J. Wan, Understanding the high activity of Fe–N–C electrocatalysts in oxygen reduction: Fe/Fe 3 C nanoparticles boost the activity of Fe–N x, J. Am. Chem. Soc. 138 (2016) 3570–3578, https://doi.org/10.1021/jacs.6b00757.
[33] J.H. Kim, Y.J. Sa, H.Y. Jeong, S.H. Joo, Roles of Fe − N x and Fe − Fe 3 C@C species in Fe − N/C electrocatalysts for oxygen reduction reaction, ACS Appl. Mater. Interfaces 9 (2017) 9567–9575, https://doi.org/10.1021/acsami.6b13417.
[34] G. Wu, A. Santandreu, W. Kellogg, S. Gupta, O. Ogoke, H. Zhang, H.-L.L. Wang, L. Dai, Carbon nanocomposite catalysts for oxygen reduction and evolution reactions: from nitrogen doping to transition-metal addition, Nano Energy 29 (2016) 83–110, https://doi.org/10.1016/j.nanoen.2015.12.032.
[35] V. Goellner, C. Baldizzone, A. Schuppert, M.T. Sougrati, K. Mayrhofer, F. Jaouen, Degradation of Fe/N/C catalysts upon high polarization in acid medium, Phys. Chem. Chem. Phys. 16 (2014) 18454–18462, https://doi.org/10.1039/C4CP02882A.
[36] G. Wu, M. Nelson, S. Ma, H. Meng, G. Cui, P.K. Shen, Synthesis of nitrogen-doped onion-like carbon and its use in carbon-based CoFe binary non-precious-metal catalysts for oxygen-reduction, Carbon N. Y. 49 (2011) 3972–3982, https://doi.org/10.1016/j.carbon.2011.05.036.
[37] N. Ramaswamy, S. Mukerjee, Influence of inner-and outer-sphere Electron transfer mechanisms during electrocatalysis of oxygen reduction in alkaline media, J. Phys. Chem. C 115 (2011) 18015–18026, https://doi.org/10.1021/jp204680p.
[38] F.E.R. Oliveira, N.A. Galiote, F.H.B. Lima, Investigation of earth-abundant oxygen reduction electrocatalysts for the cathode of passive air-breathing direct formate fuel cells, Catalysts 8 (2018) 320, https://doi.org/10.3390/catal8080320.
[39] S. Ma, G.A. Goenaga, A.V. Call, D.J. Liu, Cobalt imidazolate framework as precursor for oxygen reduction reaction electrocatalysts, Chem. - A Eur. J. 17 (2011) 2063–2067, https://doi.org/10.1002/chem.201003080.
[40] N. Ramaswamy, S. Mukerjee, Fundamental mechanistic understanding of electrocatalysis of oxygen reduction on Pt and Non-Pt surfaces: acid versus alkaline media, Adv. Phys. Chem. 2012 (2012) 1–17, https://doi.org/10.1155/2012/491604.
[41] J. Maruyama, N. Fukui, M. Kawaguchi, I. Abe, Application of nitrogen-rich amino acids to active site generation in oxygen reduction catalyst, J. Power Sources 182 (2008) 489–495, https://doi.org/10.1016/j.jpowsour.2008.04.040.
[42] J. Maruyama, I. Abe, Structure control of a carbon-based noble-metal-free fuel cell cathode catalyst leading to high power output, Chem. Commun. (2007) 2879–2881, https://doi.org/10.1039/b703723f.